THE ARCHIVE OF MECHANICAL ENGINEERING

Vol. LII 2005 Number 1

Key words: *exhaust emission, dispersion, modelling*

*KRZYSZTOF BRZOZOWSKI**)

NUMERICAL MODELLING OF CAR EXHAUST POLLUTANT DISPERSION WITH CHEMICAL REACTIONS

The paper presents a numerical model of car exhaust pollutant dispersion. The model can be used for estimation of the impact of pollutant emissions from road vehicles on the environment. The finite volume method has been used for model formulation. Equations obtained after discretisation are solved by using different methods like Runge-Kutta, Crank-Nicholson or decomposition methods. On the basis of the numerical simulation, conclusions are formulated about the numerical effectiveness of the integration methods used. In the paper, a problem of nitrogen oxides dispersion is formulated and solved, whereby chemical reactions are included in considerations.

The model presented in the paper has been used for numerical calculations of car exhaust pollutant concentrations in a real car park. The last part of the paper presents some numerical results of calculations, which include emissions after cold start of engines.

NOTATION

ϕ – concentration of pollutant at point with coordinates $(x^{(1)}, x^{(2)}, x^{(3)})$,
U – vector of wind velocity,
$\mu^{(1)}$ – turbulent diffusion coefficient,
I – the term describing sources of emission, absorption of pollutants and chemical reactions,
t – time,
t_c – calculation time,
Δt – integration step,

*) *University of Bielsko-Biała, ul. Willowa 2, 43-309 Bielsko-Biała, Poland; E-mail: kbrzozowski@ath.bielsko.pl*

ε – permissible error,
r – number of iterations,
E – percentage difference,
k_1, k_2 – reaction coefficients,
T – ambient temperature,
Q – intensity of solar radiation,
$e_{(l)}$ – road emission,
$\varepsilon_{(l)}$ – intensity of additional emission,
v – average velocity of vehicle,
V_c – engine capacity.

1. Introduction

It is obvious that road transport, including passenger cars, causes environmental damage. Road traffic, especially in urban areas, is one of the chief factors causing the atmosphere to deteriorate. The negative impact of traffic is connected, in the first place, with exhaust emissions from engines of vehicles but also with noise, dust emission and fuel evaporation [1].

Mathematical modelling of emission and dispersion of exhaust gases of moving vehicles now represents one of the important stages in the design and modernization of road infrastructure. The models are also crucial tools in managing the quality of the air in urban areas. They can be used to evaluate pollutant concentration and also to predict pollutant concentrations for different scenarios.

In order to define the state of the air around road infrastructures, a range of mathematical models have been used which differ considerably in their degree of complexity. In mathematical modelling of traffic pollutant dispersion CFD (Computer Fluid Dynamics), empirical, analytical and hybrid models are used [2].

A complex mathematical model enabling car exhaust pollutant concentration to be evaluated or predicted has the following elements:
- exhaust emission model taking into account the cold start phase,
- transport model which describes dispersion of pollutants caused by advection, turbulent diffusion and if necessary also taking into account chemical reactions,
- air flow model with proper turbulence model.

It is known that results of numerical calculations depend on input data. In modelling car exhaust pollutant concentration, calculation results obviously depend directly on the data concerning sources of emission, namely individual vehicles. The relationship of the emission (in the form of road emission or emission intensity) of individual pollutants to parameters of

vehicle motion is described by emission characteristics. The dependence of the average road emission on average vehicle velocity leads to the formulation of quasi-dynamic (static) emission characteristics. If the amount of emission is related to instantaneous vehicle velocity and acceleration, then the relationships are known as dynamic characteristics [2], [3].

Pollutant dispersion models differ significantly in the degree of complexity of the chemical reactions considered. In car exhaust pollutant dispersion models, chemical reactions of nitrogen oxides are taken into account, since these lead to ozone and thus photochemical smog.

The process of turbulent pollutant transport can be described by partial differential equations, which after discretisation on the basis of one of the most popular methods (finite difference, finite element, finite volume method) can be reduced to a set of ordinary differential equations (ODE). The solution can be obtained when information describing medium and environment is also known. This means that the solution of the problem requires information about fluid field velocity and temperature, which is possible after solution of another set of partial differential equations (energy, Navier-Stokes, continuity and turbulence model equations). The examples of those models can be found in books [2], [4]. Sometimes, however, (if terrain is flat and we take into account a boundary layer of the atmosphere) simple algebraic equations can be used.

In this paper we look only at the problem of solution of the dispersion equation (for turbulent motion) after discretization by the finite volume method. Investigations were carried out to find the best integration method of ODE in the dispersion problem. The numerical effectiveness of classic integration methods like Runge-Kutta and Crank-Nicholson [5] is compared to decomposition methods [6]. Additional investigations are carried out after including the non-linear terms describing chemical reactions in the dispersion model.

2. Advection-diffusion equation, discretisation method

The equation of pollutant dispersion can be written in the following form [2]:

$$\frac{\partial \phi}{\partial t} + \sum_{i=1}^{3} \left[\frac{\partial}{\partial x^{(i)}} (U^{(i)} \phi) - \frac{\partial}{\partial x^{(i)}} \left(\mu^{(i)} \frac{\partial \phi}{\partial x^{(i)}} \right) \right] = I. \tag{1}$$

Discretisation of equation (1) by finite volume method [7] allows us to reduce a problem of solution of a partial differential equation for four variables

$(t, x^{(1)}, x^{(2)}, x^{(3)})$ to the problem of solving an ordinary differential equation. The finite domain V, in which we seek to define values of function ϕ, can be divided into prismatic elements shown in Fig. 1.

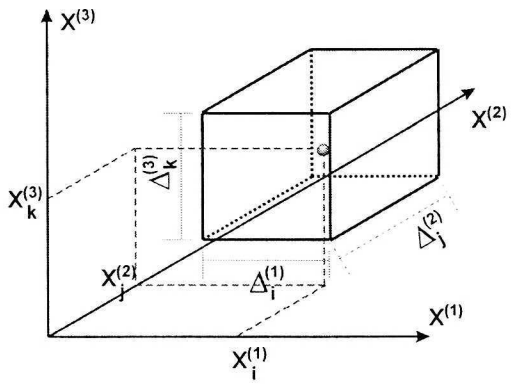

Fig. 1. Elementary rectangular prism with volume $V_{i,j,k}$

The ends of the intervals with nodal points $x_1^{(l)}, x_2^{(l)}, \ldots, x_{n_l}^{(l)}$ for $l = 1, 2, 3$; are denoted in the way presented in Fig. 2 with indices $\pm\frac{1}{2}$.

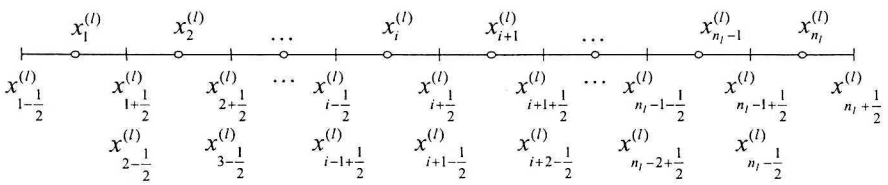

Fig. 2. Nodal points $x_1^{(l)} \div x_{n_l}^{(l)}$ and denotations of end points of intervals for $i = 1, \ldots, n_l$; $l = 1, 2, 3$

It is also assumed that inside prism $V_{i,j,k}$, concentration of pollutants is constant with reference to spatial coordinates, that is

$$\phi = \phi_{i,j,k}(t) \quad \text{for} \quad (x^{(1)}, x^{(2)}, x^{(3)}) \in V_{i,j,k}. \tag{2}$$

Elementary volume is:

$$V_{i,j,k} = \Delta_i^{(1)} \Delta_j^{(2)} \Delta_k^{(3)}. \tag{3}$$

After integrating equation (1) over elementary volume $V_{i,j,k}$ we obtain

$$\int_{V_{i,j,k}} \frac{\partial \phi}{\partial t} dV + \int_{V_{i,j,k}} \frac{\partial}{\partial x^{(1)}}(U^{(1)}\phi) dV - \int_{V_{i,j,k}} \frac{\partial}{\partial x^{(1)}}\left(\mu^{(1)} \frac{\partial \phi}{\partial x^{(1)}}\right) dV$$
$$+ \int_{V_{i,j,k}} \frac{\partial}{\partial x^{(2)}}(U^{(2)}\phi) dV - \int_{V_{i,j,k}} \frac{\partial}{\partial x^{(2)}}\left(\mu^{(2)} \frac{\partial \phi}{\partial x^{(2)}}\right) dV \tag{4}$$
$$+ \int_{V_{i,j,k}} \frac{\partial}{\partial x^{(3)}}(U^{(3)}\phi) dV - \int_{V_{i,j,k}} \frac{\partial}{\partial x^{(3)}}\left(\mu^{(3)} \frac{\partial \phi}{\partial x^{(3)}}\right) dV = \int_{V_{i,j,k}} I dV.$$

Paper [2] presents a detailed description of algorithms allowing calculation of integrals from equation (4) by using different stability approximation schemes [8] and different forms of boundary conditions.

The set of ODE equations which we obtain after discretisation, taking into account boundary conditions, can be written in the form [2]

$$\frac{d\phi_{i,j,k}}{dt} + a^{(1)}_{i,j,k} + \sum_{l=\max\{i-2,1\}}^{\min\{i+2, n^{(1)}_{j,k}\}} \alpha^{(1)}_{i,j,k,l}\, \phi_{l,j,k}$$
$$+ a^{(2)}_{i,j,k} + \sum_{l=\max\{j-2,1\}}^{\min\{j+2, n^{(2)}_{i,k}\}} \alpha^{(2)}_{i,j,k,l}\, \phi_{i,l,k} \tag{5}$$
$$+ a^{(3)}_{i,j,k} + \sum_{l=\max\{k-2,1\}}^{\min\{k+2, n^{(3)}_{i,j}\}} \alpha^{(3)}_{i,j,k,l}\, \phi_{i,j,l} = I_{i,j,k},$$

where $a^{(ml)}_{i,j,k}$, $\alpha^{(1)}_{i,j,k,l}$, $\alpha^{(2)}_{i,j,k,l}$, $\alpha^{(3)}_{i,j,k,l}$ can be found in [2], [4].

Further considerations will be limited to the case when the domain investigated is a rectangular prism, for which the assumption of the vector of unknowns (values of function ϕ at points of discretisation) has the form

$$\boldsymbol{\phi} = [\phi_{1,1,1}, ..., \phi_{n_1,1,1}, ..., \phi_{i,j,k}, ..., \phi_{n_1,n_2,n_3}]^T, \tag{6}$$

with $n = n_1 \cdot n_2 \cdot n_3$ components, where n_l is a number of division intervals in direction $l = 1, 2, 3$.

Equations (5) are a set of n first order ordinary differential equations according to variable t, which can also be written in a matrix form

$$\frac{d\boldsymbol{\phi}}{dt} + \boldsymbol{\Lambda}(\boldsymbol{\phi}) = \mathbf{f}, \tag{7.1}$$

where

$$\Lambda(\phi)_{i,j,k} = \sum_{l=\max\{i-2,1\}}^{\min\{i+2,n_1\}} \alpha^{(1)}_{i,j,k,l}\phi_{l,j,k} + \sum_{l=\max\{j-2,1\}}^{\min\{j+2,n_2\}} \alpha^{(2)}_{i,j,k,l}\phi_{i,l,k} + \sum_{l=\max\{k-2,1\}}^{\min\{k+2,n_3\}} \alpha^{(3)}_{i,j,k,l}\phi_{i,j,l},$$

$$\mathbf{f} = [f_{1,1,1}, \ldots, f_{n_1,1,1}, \ldots, f_{i,j,k}, \ldots, f_{n_1,n_2,n_3}]^T, \; f_{i,j,k} = I_{i,j,k} - \sum_{l=1}^{3} a^{(l)}_{i,j,k}.$$

In order to solve equations (7), appropriate initial conditions have to be used. Usually it can be assumed that

$$\boldsymbol{\phi}(t_0) = \boldsymbol{\phi}^{(0)}, \tag{7.2}$$

which means that concentration of pollutant $\boldsymbol{\phi}^{(0)}$ in time t_0 is known; this is usually equal to background concentration.

3. Methods of solving equations after discretisation

The solution of the initial problem in form (7) can be obtained by different numerical methods. The most popular are the Runge-Kutta method (especially of IV order) and multi-step (extrapolation and interpolation) methods. Description of these methods can be found in books on numerical methods like [5], [9], [10]. The problem formulated by equations (7) can also be solved also by using one of the classic methods for parabolic equations such as the implicit and explicit method or the Crank-Nicholson method [5], [7].

The Runge-Kutta (of IV order) and Crank-Nicholson methods are described below. Both methods can be used for integrating linear and non-linear differential equations.

After assuming $t_0 = 0$, the initial equations (7) can be written in the form

$$\dot{\boldsymbol{\phi}} = \mathbf{F}(t, \boldsymbol{\phi}), \tag{8.1}$$

$$\boldsymbol{\phi}(0) = \boldsymbol{\phi}^0, \tag{8.2}$$

where $\mathbf{F}(t, \boldsymbol{\phi}) = \mathbf{f} - \boldsymbol{\Lambda}(\boldsymbol{\phi})$.

If we denote

$$\boldsymbol{\phi}^s = \boldsymbol{\phi}(s \cdot \Delta t), \tag{9.1}$$

$$\mathbf{f}^s = \mathbf{f}(s \cdot \Delta t), \tag{9.2}$$

$$\mathbf{F}^s = \mathbf{F}(s \cdot \Delta t), \tag{9.3}$$

for known $\boldsymbol{\phi}^s$, in Runge-Kutta method the solution of $\boldsymbol{\phi}^{s+1}$ is found by solving equation [5], [10]

$$\boldsymbol{\phi}^{s+1} = \boldsymbol{\phi}^s + \frac{1}{6}[\mathbf{K}_1 + 2\mathbf{K}_2 + 2\mathbf{K}_3 + \mathbf{K}_4] \tag{10}$$

where

$$\mathbf{K}_1 = \Delta t \cdot \mathbf{F}(s \cdot \Delta t, \boldsymbol{\phi}^s), \quad \mathbf{K}_2 = \Delta t \cdot \mathbf{F}\left(\left(s + \frac{1}{2}\right) \cdot \Delta t, \boldsymbol{\phi}^s + \frac{1}{2}\mathbf{K}_1\right),$$

$$\mathbf{K}_3 = \Delta t \cdot \mathbf{F}\left(\left(s + \frac{1}{2}\right) \cdot \Delta t, \boldsymbol{\phi}^s + \frac{1}{2}\mathbf{K}_2\right), \quad \mathbf{K}_4 = \Delta t \cdot \mathbf{F}((s+1) \cdot \Delta t, \boldsymbol{\phi}^s + \mathbf{K}_3).$$

The method gives an error of the order $(\Delta t)^4$, so the result will be found with a good accuracy. The Runge-Kutta method can be also used for integrating stiff ODE, which we find in fluid dynamics [11]. In the R-K method, it is necessary to use a small integration step. In some cases, a disadvantage of R-K method is multiple (four times) calculation of vector $\mathbf{F}$, in one integration step, in order to find the solution of $\boldsymbol{\phi}^{s+1}$ from (10). It increases the calculation time.

In the Crank-Nicholson method used for solving problem (7), it is assumed that solution of $\boldsymbol{\phi}^{s+1}$ can be obtained from equation

$$\frac{\boldsymbol{\phi}^{s+1} - \boldsymbol{\phi}^s}{\Delta t} = \frac{1}{2}[-\boldsymbol{\Lambda}(\boldsymbol{\phi}^{s+1}) + \mathbf{f}^{s+1} - \boldsymbol{\Lambda}(\boldsymbol{\phi}^s) + \mathbf{f}^s]. \tag{11}$$

The left side of equation (11) is a discrete approximation of $\frac{d\boldsymbol{\phi}}{dt}$, by using central difference for $t = \left(s + \frac{1}{2}\right)\Delta t$. The right side of equation (11) is equal to average values of vector $\mathbf{F}$ in (8), for layers s and $s+1$.

From equation (11) we can obtain

$$\boldsymbol{\phi}^{s+1} = \boldsymbol{\phi}^s - \frac{\Delta t}{2}\boldsymbol{\Lambda}(\boldsymbol{\phi}^{s+1}) + \frac{\Delta t}{2}\mathbf{f}^{s+1} - \frac{\Delta t}{2}\boldsymbol{\Lambda}(\boldsymbol{\phi}^s) + \frac{\Delta t}{2}\mathbf{f}^s. \tag{12}$$

If we assume operator $\boldsymbol{\Lambda}$ as a sum of linear and non-linear terms we can write

$$\boldsymbol{\Lambda}(\boldsymbol{\phi}) = \mathbf{A} \cdot \boldsymbol{\phi} + \mathbf{B}(\boldsymbol{\phi}), \tag{13}$$

where $\mathbf{A}$ is the square matrix and $\mathbf{B}$ is the non-linear term.

After assuming (13) from equation (12) we can obtain

$$\boldsymbol{\phi}^{s+1} = -\frac{\Delta t}{2}\mathbf{A} \cdot \boldsymbol{\phi}^{s+1} + \mathbf{g}(\boldsymbol{\phi}^{s+1}) + \mathbf{G}^{s}, \tag{14}$$

where $\mathbf{g}(\boldsymbol{\phi}^{s+1}) = \frac{-\Delta t}{2}\mathbf{B}(\boldsymbol{\phi}^{s+1})$, $\mathbf{G}^{s} = \boldsymbol{\phi}^{s} - \frac{\Delta t}{2}\boldsymbol{\Lambda}(\boldsymbol{\phi}^{s}) + \frac{\Delta t}{2}[\mathbf{f}^{s+1} + \mathbf{f}^{s}]$,
and in the next step

$$\mathbf{M} \cdot \boldsymbol{\phi}^{s+1} = \mathbf{g}(\boldsymbol{\phi}^{s+1}) + \mathbf{G}^{s} \tag{15}$$

where $\mathbf{M} = \mathbf{I} + \frac{\Delta t}{2}\mathbf{A}$.

If the non-linear term $\mathbf{B}$ of operator $\boldsymbol{\Lambda}$ exists, then equations (15) are a set of n non-linear algebraic equations. If operator $\boldsymbol{\Lambda}$ is linear, the equations (15) are a set of linear algebraic equations and $\boldsymbol{\phi}^{s+1}$ can be determined

$$\boldsymbol{\phi}^{s+1} = \mathbf{M}^{-1} \cdot \mathbf{G}^{s}. \tag{16}$$

Computing of matrix $\mathbf{M}^{-1}$ is numerically efficient for the case of $\mathbf{M}$ with constant coefficients. Unfortunately, in most cases $\mathbf{M}$ does not have constant coefficients. Solving equations (15) for each integration step by elimination methods is not efficient numerically, either. Better numerical efficiency can be achieved using one of the iterative methods, both for linear and non-linear operator $\boldsymbol{\Lambda}$.

After decomposing matrix $\mathbf{M}$ to the form

$$\mathbf{M} = \mathbf{D} + \mathbf{R}, \tag{17}$$

where $\mathbf{D}$ is diagonal matrix, with elements $d_{ii} = m_{ii}$ for $i = 1, ..., n$; equations (15) can be written in the form

$$\mathbf{D} \cdot \boldsymbol{\phi}^{s+1} = \mathbf{H}(\boldsymbol{\phi}^{s+1}) + \mathbf{G}^{s}, \tag{18}$$

where $\mathbf{H}(\boldsymbol{\phi}^{s+1}) = -\mathbf{R} \cdot \boldsymbol{\phi}^{s+1} + \mathbf{g}(\boldsymbol{\phi}^{s+1})$.

The most popular method, which can be used for solving equations (18), is the iterative Gauss-Seidel method. If we denote $\boldsymbol{\phi}^{(r)}$ as r-th approximation of vector $\boldsymbol{\phi}^{s+1}$ and we know approximation $\boldsymbol{\phi}^{(r-1)}$, the components of vectors $\boldsymbol{\phi}^{(r)}$ can be calculated

$$\phi_i^{(r)} = \frac{1}{d_{ii}}\left[\mathbf{H}\left(\phi_1^{(r)}, ..., \phi_{i-1}^{(r)}, \phi_i^{(r-1)}, ..., \phi_n^{(r-1)}\right) + \mathbf{G}^s\right] \text{ for } i = 1, 2, ..., n;\ r = 1, 2, ... \tag{19}$$

It is also assumed that $\boldsymbol{\phi}^{(0)} = \boldsymbol{\phi}^s$.
The iteration procedure has to be repeated until the following stop condition is fulfilled

$$\left| \frac{\|\boldsymbol{\phi}^{(r)}\| - \|\boldsymbol{\phi}^{(r-1)}\|}{\|\boldsymbol{\phi}^{(r)}\|} \right| < \varepsilon, \tag{20}$$

where ε is permissible error.

It is possible to formulate stop conditions by limiting the number of iterations, that is conditions $r \leq r_{\max}$, where $r_{\max}$ is maximal number of iterations. However, using small values $r_{\max}$ can lead to inadequate calculation results.

The Crank-Nicholson method gives an error of the order $(\Delta t)^2$, assuming that equations (18) are solved with good accuracy.

The integration methods above do not take into account a special form of operator $\boldsymbol{\Lambda}$ in the advection-diffusion equation. The method of decomposing the advection-diffusion equation with respect to successive variables was presented in [6]. In this method, two schemes can be used to solve equations (7): one and two-cycle schemes. Both schemes are unconditionally stable and enable us to find the solution of the problem with high numerical efficiency. Below, both methods are applied to solving equations (7).

The dispersion equation (1) can also be written in the form

$$\frac{\partial \phi}{\partial t} + A_1\phi + A_2\phi + A_3\phi = I, \tag{21}$$

where $A_l\phi = \dfrac{\partial}{\partial x^{(l)}}(U^{(l)}\phi) - \dfrac{\partial}{\partial x^{(l)}}\left(\mu^{(l)}\dfrac{\partial \phi}{\partial x^{(l)}}\right)$, for $l = 1, 2, 3$.

Discrete approximations of $A_1\phi$, $A_2\phi$, $A_3\phi$ in accordance with (5) are

$$\Lambda_{1,i,j,k} = a_{i,j,k}^{(1)} + \sum_{l=\max\{i-2,1\}}^{\min\{i+2, n_{j,k}^{(1)}\}} \alpha_{i,j,k,l}^{(1)}\,\phi_{l,j,k}, \tag{22.1}$$

$$\Lambda_{2,i,j,k} = a_{i,j,k}^{(2)} + \sum_{l=\max\{j-2,1\}}^{\min\{j+2, n_{i,k}^{(2)}\}} \alpha_{i,j,k,l}^{(2)}\,\phi_{i,l,k}, \tag{22.2}$$

$$\Lambda_{3,i,j,k} = a^{(3)}_{i,j,k} + \sum_{l=\max\{k-2,1\}}^{\min\{k+2,n^{(3)}_{i,j}\}} \alpha^{(3)}_{i,j,k,l}\,\phi_{i,j,l}. \tag{22.3}$$

If the discrete approximation of equation (21) is written in the form

$$\frac{d\boldsymbol{\phi}}{dt} + \boldsymbol{\Lambda}_1(\boldsymbol{\phi}) + \boldsymbol{\Lambda}_2(\boldsymbol{\phi}) + \boldsymbol{\Lambda}_3(\boldsymbol{\phi}) = \mathbf{f}, \tag{23}$$

where $\boldsymbol{\Lambda}_1, \boldsymbol{\Lambda}_2, \boldsymbol{\Lambda}_3$ are defined in (22), $\mathbf{f}$ is defined in (7.1), in accordance with [6], the method of decomposing equation (23) with respect to successive variables can be applied.

If we know $\boldsymbol{\phi}^s$, that is components of vector $\boldsymbol{\phi}$ on layer s (in relation to time), for the one-cycle scheme $\boldsymbol{\phi}^{s+1}$ is found by solving the following sequence of problems [6]

$$\frac{\boldsymbol{\phi}^{s+1/3} - \boldsymbol{\phi}^s}{\Delta t} + \boldsymbol{\Lambda}_3\left(\frac{\boldsymbol{\phi}^{s+1/3} + \boldsymbol{\phi}^s}{2}\right) = \mathbf{f}^{s+1/2}, \tag{24.1}$$

$$\frac{\boldsymbol{\phi}^{s+2/3} - \boldsymbol{\phi}^{s+1/3}}{\Delta t} + \boldsymbol{\Lambda}_2\left(\frac{\boldsymbol{\phi}^{s+2/3} + \boldsymbol{\phi}^{s+1/3}}{2}\right) = 0, \tag{24.2}$$

$$\frac{\boldsymbol{\phi}^{s+1} - \boldsymbol{\phi}^{s+2/3}}{\Delta t} + \boldsymbol{\Lambda}_1\left(\frac{\boldsymbol{\phi}^{s+1} + \boldsymbol{\phi}^{s+2/3}}{2}\right) = 0. \tag{24.3}$$

Solution with the one-cycle decomposition scheme gives an error of the order Δt [6].

When we use the two-cycle scheme, the vector $\boldsymbol{\phi}^{s+1}$ can be obtained by solution of the following systems of equations [6]

$$\frac{\boldsymbol{\phi}^{s+1/6} - \boldsymbol{\phi}^s}{\Delta t} + \frac{1}{2}\boldsymbol{\Lambda}_1^{s+3/6}\left(\frac{\boldsymbol{\phi}^{s+1/6} + \boldsymbol{\phi}^s}{2}\right) = 0, \tag{25.1}$$

$$\frac{\boldsymbol{\phi}^{s+2/6} - \boldsymbol{\phi}^{s+1/6}}{\Delta t} + \frac{1}{2}\boldsymbol{\Lambda}_2^{s+3/6}\left(\frac{\boldsymbol{\phi}^{s+2/6} + \boldsymbol{\phi}^{s+1/6}}{2}\right) = 0, \tag{25.2}$$

$$\frac{\boldsymbol{\phi}^{s+3/6} - \boldsymbol{\phi}^{s+2/6}}{\Delta t} + \frac{1}{2}\boldsymbol{\Lambda}_3^{s+3/6}\left(\frac{\boldsymbol{\phi}^{s+3/6} + \boldsymbol{\phi}^{s+2/6}}{2}\right) = \frac{1}{2}\mathbf{f}^{s+3/6}, \tag{25.3}$$

$$\frac{\boldsymbol{\phi}^{s+4/6} - \boldsymbol{\phi}^{s+3/6}}{\Delta t} + \frac{1}{2}\boldsymbol{\Lambda}_3^{s+3/6}\left(\frac{\boldsymbol{\phi}^{s+4/6} + \boldsymbol{\phi}^{s+3/6}}{2}\right) = \frac{1}{2}\mathbf{f}^{s+3/6}, \tag{25.4}$$

$$\frac{\boldsymbol{\phi}^{s+5/6} - \boldsymbol{\phi}^{s+4/6}}{\Delta t} + \frac{1}{2}\boldsymbol{\Lambda}_2^{s+3/6}\left(\frac{\boldsymbol{\phi}^{s+5/6} + \boldsymbol{\phi}^{s+4/6}}{2}\right) = 0, \tag{25.5}$$

$$\frac{\boldsymbol{\phi}^{s+1} - \boldsymbol{\phi}^{s+5/6}}{\Delta t} + \frac{1}{2}\boldsymbol{\Lambda}_1^{s+3/6}\left(\frac{\boldsymbol{\phi}^{s+1} + \boldsymbol{\phi}^{s+5/6}}{2}\right) = 0, \tag{25.6}$$

Solution with the two-cycle decomposition scheme gives an error of the order $(\Delta t)^2$, so accuracy is equal to that obtained by the Crank-Nicholson method.

In the next part of the paper all integration methods described are tested with respect to accuracy for different integration time step and numerical efficiency. Two different problems were formulated and solved:
- the first is connected with the dispersion process given by equations (7),
- the second is formulated for dispersion with chemical reactions of pollutants, which leads to a multiplication of the number of equations and makes the dispersion problem non-linear.

The dispersion problem, which takes into account chemical changes, uses the model of chemical reactions of nitrogen oxides given in [2], [12], [13]

$$\begin{aligned} NO + O_3 &\xrightarrow{k_1} NO_2 + O_2 \\ NO_2 + h\nu &\xrightarrow{k_2} NO + O \\ O^{\bullet} + O_2 &\longrightarrow O_3 \end{aligned} \tag{26.1}$$

Mathematical description of this model is a set of the following non-linear ODEs

$$\begin{cases} \dfrac{d\phi_{NO}}{dt} = k_2\phi_{NO_2} - k_1\phi_{O_3}\phi_{NO} \\ \dfrac{d\phi_{NO_2}}{dt} = k_1\phi_{NO}\phi_{O_3} - k_2\phi_{NO_2} \\ \dfrac{d\phi_{O_3}}{dt} = k_2\phi_{NO_2} - k_1\phi_{NO}\phi_{O_3} \end{cases} \tag{26.2}$$

In the paper this model is applied in the advection-diffusion equation in the manner described below. We assumed that advection-diffusion equations for reactive pollutants have the form

$$\frac{d\phi_c}{dt} + \Lambda(\phi_c) = I_c \quad \text{for} \quad c = 1, 2, 3..., n_c, \tag{27}$$

where n_c is the number of pollutants which are taken into account in dispersion modelling.

In order to consider the model of reaction with nitrogen oxides $n_c = 3$, it is assumed

$$\phi_1 = \phi_{NO}, \tag{28.1}$$

$$\phi_2 = \phi_{NO_2}, \tag{28.2}$$

$$\phi_3 = \phi_{O_3}. \tag{28.3}$$

In source terms I_c we have to add respectively

$$I_1 : k_2\phi_2 - k_1\phi_3\phi_1, \tag{29.1}$$

$$I_2 : k_1\phi_1\phi_3 - k_2\phi_2, \tag{29.2}$$

$$I_3 : k_2\phi_2 - k_1\phi_1\phi_3, \tag{29.3}$$

The discretisation method for equations (27) is exactly the same as for a single pollutant. The essential difference in relation to single pollutant dispersion modelling is that the equations (27) are directly conjugate with chemical reactions. The equations (27) can be written in the form

$$\frac{d\phi_c}{dt} + \Lambda(\phi_c) = f_c(\phi_1, \phi_2, \phi_3) \quad \text{for} \quad c = 1, 2, 3. \tag{30}$$

As it can be seen in dispersion modelling of nitrogen oxides with the chemical reaction model, we obtain three times more (3n) partial differential equations (30) than for a single pollutant. The integration algorithm can be completed by additional conditions

$$\phi_{c,i,j,k} \geq 0. \tag{31}$$

It should be noted that non-linearity of equations (26) results in non-linearity of equations (30).

4. Analysis of numerical efficiency

Analysis of numerical efficiency of methods used for integration of ODEs after finite volume discretisation has been performed for the rectangular prism presented in Fig. 3. The domain investigated was divided into elements with a volume of $1 \times 0.5 \times 0.1$ m. After discretisation with $n_1 = n_2 = 40$; $n_3 = 100$ we have $n = 160000$ control volumes.

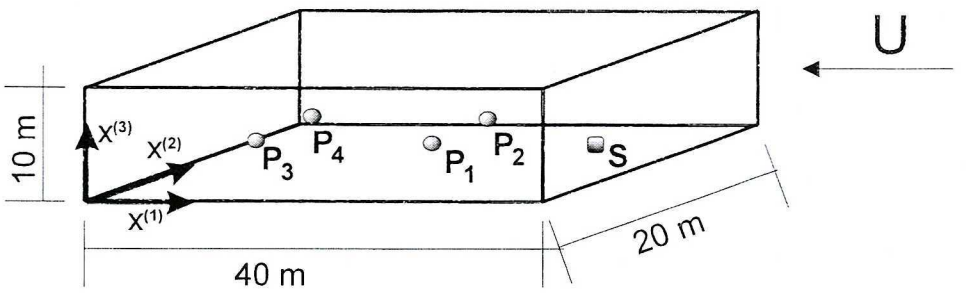

Fig. 3. Domain investigated: S – emission source, $P_1 \div P_4$ – points inside domain in which pollutant concentrations ϕ are investigated

The emission source with maximum emission intensity $f_{\max}$ equal to 100 mg/s is located inside the domain at $x^{(1)} = 35$; $x^{(2)} = 10$, at height $x^{(3)} = 1$ m. The source function is assumed to be a triangular function (Fig. 4a)

$$f = \begin{cases} 0 & \text{if} \quad t < t_s \\ f_{\max} \dfrac{t}{t_m} & \text{if} \quad t \leq t_m \\ f_{\max} \left(1 - \dfrac{t - t_m}{t_k - t_m} \right) & \text{if} \quad t_m < t \leq t_k \\ 0 & \text{if} \quad t > t_k \end{cases} \tag{32}$$

This means that, for volume $V_{i,j,k}$ surrounding the emission source, term $I_{i,j,k}$ has the form

$$I_{i,j,k} = \frac{1}{V_{i,j,k}} f. \tag{33}$$

Additionally, we assumed the start emission time $t_s = 0$. Maximum emission occurs for $t_m = 20$ s and stop of emission is at time $t_k = 40$ s.

The direction of air velocity vector was $\alpha = 180°$ in relation to axis $OX^{(1)}$ with velocity $U = 3$ m/s at height 14 m (Fig. 4b). The vertical distribution of

the air velocity was obtained from the pre-processor for neutral conditions of the atmosphere [2]. It was also assumed that the velocity vector has components $U^{(1)} = U(x^{(3)})$, $U^{(2)} = U^{(3)} = 0$.

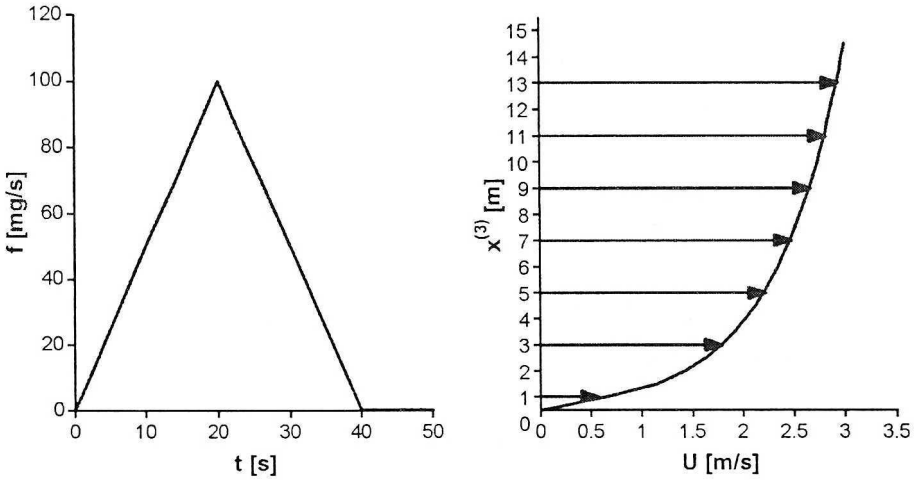

Fig. 4. Input calculation data: a) emission intensity of source S; b) vertical distribution of air velocity U

Calculations have been carried out with all methods described in the paper. The results obtained for four different points P_i ($i = 1, 2, 3, 4$) inside the domain are compared.

Points P_1 (20,10,1) and P_3 (35,10,1) are located inline with the source (parallel to direction of air velocity vector), in contrast to points P_2 (20,15,1.5) and P_4 (35,15,1.5), which are located higher and outside the line connecting source and points P_1 and P_3 (see Fig. 3). Calculations assume the second kind of boundary conditions for $x^{(1)} = 40$ (inlet plane) and $x^{(3)} = 0$ (pollutant reflection). For other boundaries, conditions of the first kind are assumed. Initial concentrations inside the domain and background concentrations have been assumed as equal to zero.

Calculations were carried out by using different methods with a constant time step within time interval $t \in \langle 0,120 \rangle$ s. In calculations the following were used:

- one-cycle decomposition scheme (J),
- two-cycle decomposition scheme (D),
- Crank-Nicholson method with Gauss-Seidel iteration ($C - N$),
- Runge-Kutta (IV order) method ($R - K$).

Results obtained by different methods were compared with results obtained by the Runge-Kutta method, because this method gives the best accuracy, with a relatively small time integration step.

4.1 Linear advection-diffusion equation

The numerical simulations enabled us to find the length of time step which guarantees a good accuracy of calculation results obtained for R-K method. For this method, acceptable accuracy is obtained for integration time step $\Delta t \leq 0.05$ s. If we decrease the time step, the calculation time increases but accuracy of the results does not change. Fig. 5 and Fig. 6 present calculated pollutant concentrations in time, for points $P_1 \div P_4$ obtained by R-K methods and for integration time step $\Delta t = 0.01$ s.

Fig. 5 presents changes of pollutant concentration for points P_1 and P_3 located inline with source of emission. We can observe higher concentration at point P_1, where distance from source is smaller than from point P_3. The shapes of concentration lines for both points are similar. Differences in values are due to different distance from the source and by the turbulent diffusion process.

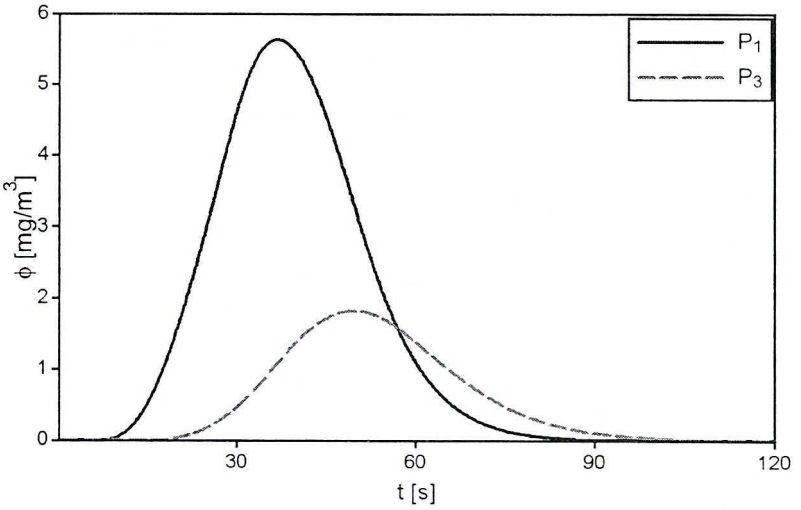

Fig. 5. Pollutant concentration at point P_1 and P_3

Fig. 6 presents calculation results for points P_2 and P_4, which are located higher and outside the axis of air motion.

Results of calculations presented in Fig. 6 differ from those in Fig. 5. The maximal concentrations are smaller than those for points P_1 and P_3, which are located in the axis of air motion. It can be noticed that smaller concentrations are observed at point P_2, which is located in an area where advection has a crucial influence on pollutant transport. For a longer distance from the source, especially outside the axis of air motion, the influence of turbulent diffusion on pollutant transport increases.

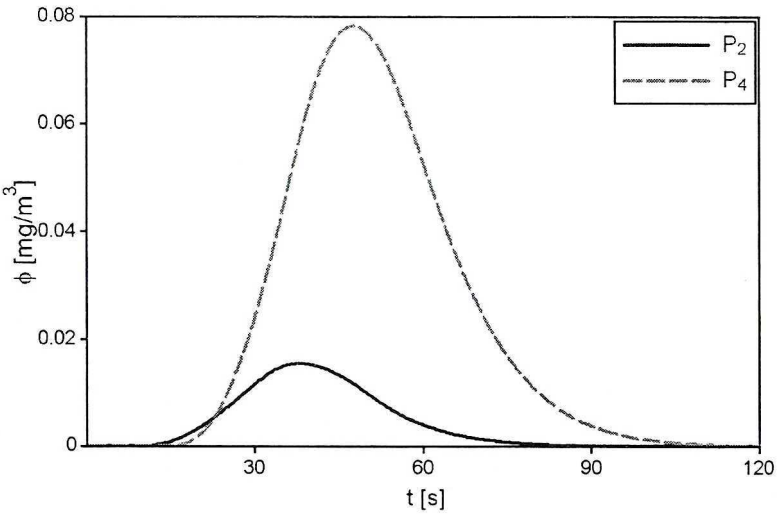

Fig. 6. Pollutant concentration at point P_2 and P_4

The comparison of accuracy of results obtained by using different methods requires calculations for different time step values. In the paper, results of calculations for time steps $\Delta t = 1$ s, $\Delta t = 0.5$ s, $\Delta t = 0.1$ s and $\Delta t = 0.05$ s and different methods are compared with results obtained by the Runge-Kutta method and time step $\Delta t = 0.01$ s.

Maximal concentration ϕ_m calculated at points $P_1 \div P_4$ by the Crank-Nicholson method and decomposition schemes are compared with those obtained for Runge-Kutta. Percentage difference is defined as

$$E = \frac{|\phi_m - \phi_{R-K}|}{\phi_{R-K}} \cdot 100\%, \tag{35}$$

where ϕ_{R-K} the value calculated by using the Runge-Kutta method, ϕ_m the value calculated by using one of the methods investigated. Fig. 7 presents percentage difference E according to (35).

The values of percentage differences presented in Fig. 7 show good correspondence for a time step less than $\Delta t = 0.5$ s. We can see the lower accuracy of the one-cycle scheme and very close results obtained for the two-cycle scheme and Crank-Nicholson method (after using value of permissible error $\varepsilon = 1e^{-6}$ in (20)). In the Crank-Nicholson method, the value of permissible error influences not only the accuracy of results (Fig. 7 results for $\varepsilon = 1e^{-6}$ and $\varepsilon = 1e^{-3}$), but also the number of iterations and, in consequence, the calculation time.

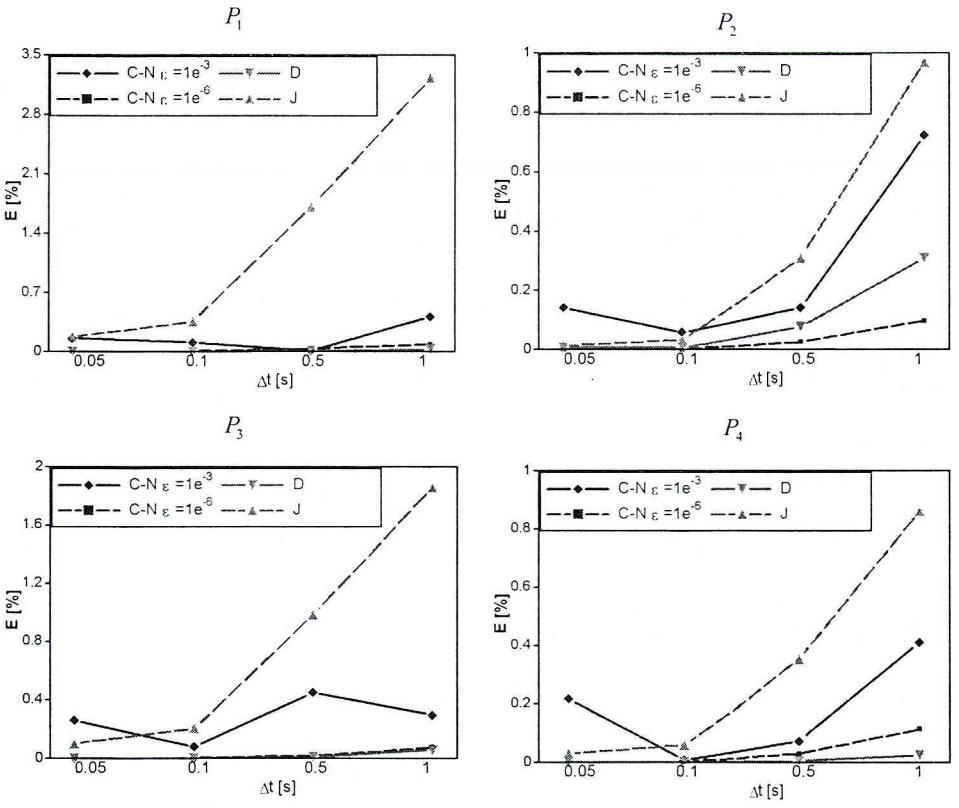

Fig. 7. Percentage difference E for maximal concentration value obtained by different methods (C-N for Crank-Nicholson, J for one-cycle scheme and D for two-cycle scheme) at points $P_1 \div P_4$

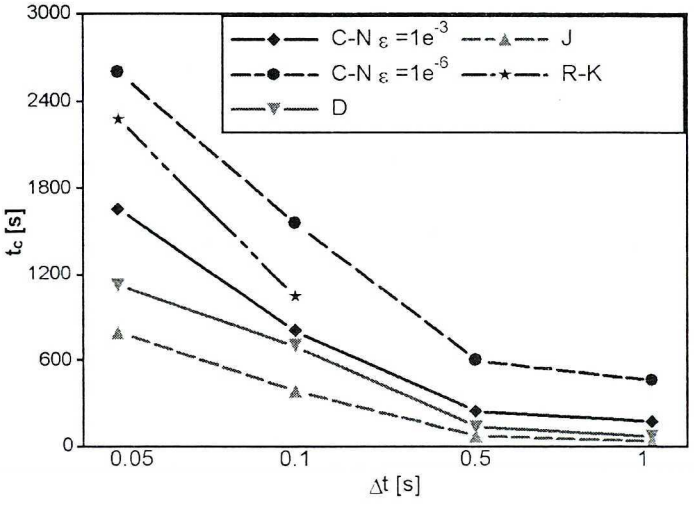

Fig. 8. Comparison of time t_c required to obtain solution
(C-N for Crank-Nicholson, R-K for Runge-Kutta, J for one-cycle scheme and D for two-cycle scheme)

Comparison of global calculation time t_c for different methods and time steps is presented in Fig. 8.

Figs. 7 and 8 show that the two-cycle decomposition scheme and the Crank-Nicholson method give the best relation between accuracy of results and calculation time.

4.2 The set of non-linear advection-diffusion equations

In this part of the paper, we investigate the numerical efficiency of different methods used for solving the non-linear advection-diffusion equations in form (30), which are conjugate with chemical reactions. It can be noticed that nitrogen dioxide (NO_2) is a pollutant which can significantly damage human respiratory system. Because nitrogen dioxide is formed in the atmosphere through the oxidation of nitrogen oxide (NO) by ozone (O_3), our investigations focus on interaction between concentration of NO_2 and O_3. Change in NO concentration is similar to that of O_3 concentration, thus, NO concentration is not presented.

All pollutant concentrations are calculated according to the model of chemical reaction presented, using the same domain. It was assumed that intensity of nitrogen oxides emission is known and 95% of the mass emitted is nitrogen oxide and 5% is emission of nitrogen dioxide.

It is assumed that background concentrations of both pollutants and the background concentration of the product of chemical reaction, ozone, are equal to zero. Reaction coefficients k_1, k_2 from (26) are dependent on ambient temperature T (288 K was assumed) and intensity of solar radiation Q (660 W/m^2 was assumed) according to paper [14]

$$k_1 = \frac{16.33}{T} e^{-\frac{1430}{T}} \; [1/ppb\ s], \tag{36}$$

$$k_2 = 0.8 \cdot 10^{-3} e^{-\frac{10}{Q} + 7.4 \cdot 10^{-6} Q} \; [1/s]. \tag{37}$$

As for single pollutant dispersion, at first we found the proper length of time step which can guarantee a good accuracy of calculation results. For the Runge-Kutta method, acceptable accuracy is obtained for integration time step $\Delta t = 0.01$ s.

Fig. 9 presents changes of pollutant concentration of NO_2 and O_3 for point $P_1 \div P_4$ obtained by R-K methods and for integration time step $\Delta t = 0.01$ s.

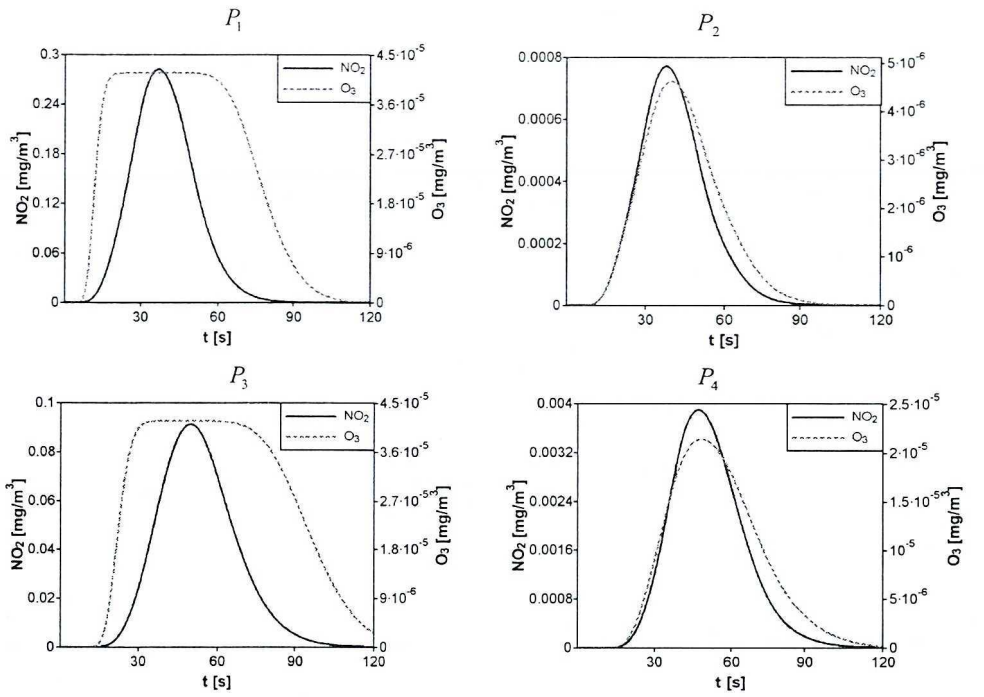

Fig. 9. Concentration of NO_2 and O_3 at points $P_1 \div P_4$

Different ozone concentrations can be seen. At points P_1 and P_3, the reaction of ozone production lasts longer and ozone concentration reaches a maximum earlier than NO_2 concentration. Ozone concentration remains constant at the time point at which concentration of NO_2 decreases to about 50% of its maximum value. At points P_2 and P_4, which are located outside the axis of main air motion, the intensity of ozone production is smaller as the result of lower NO_2 concentration. The decrease of ozone concentration is in simple relation to the decrease of NO_2 concentration.

The set of non-linear equations describing nitrogen oxides dispersion was solved by the methods presented in the paper, for different time steps: $\Delta t = 1$ s, $\Delta t = 0.5$ s, $\Delta t = 0.1$ s and $\Delta t = 0.05$ s. The results obtained for NO_2 concentrations are compared with those obtained by the Runge-Kutta method for time step $\Delta t = 0.01$ s. Maximal concentration ϕ_{NO_2} calculated at points $P_1 \div P_4$ by the Runge-Kutta and Crank-Nicholson methods and the decomposition scheme are compared using percentage difference value E defined in (35). Comparison of percentage difference values for the above methods is presented in Fig. 10.

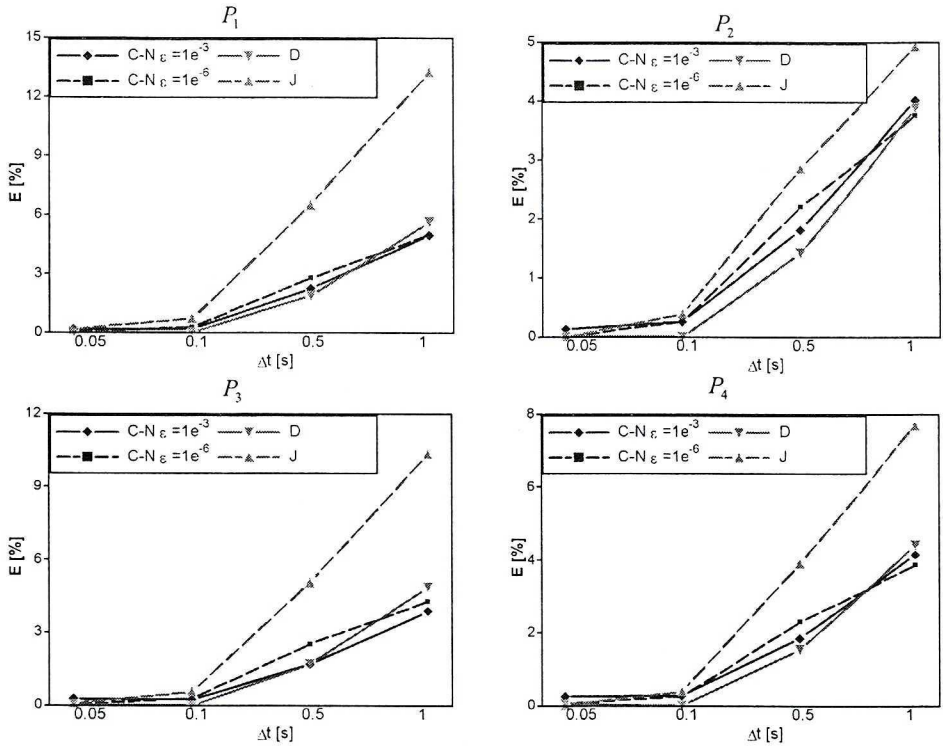

Fig. 10. Percentage difference E for maximal concentration value of NO_2 obtained by different methods (C-N for Crank-Nicholson, J for one-cycle scheme and D for two-cycle scheme) at points $P_1 \div P_4$

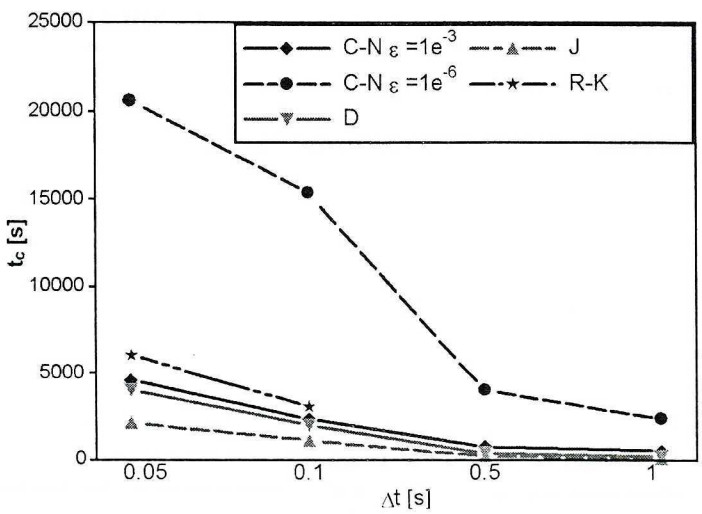

Fig. 11. Comparison of calculation time t_c
(C-N for Crank-Nicholson, R-K for Runge-Kutta, J for one-cycle scheme and D for two-cycle scheme)

The analysis of percentage difference presented in Fig. 10 shows weak correspondence for time step $\Delta t = 0.5$ s (for single pollutant dispersion this time step was sufficient). Decreasing the time integration step gives better correspondence with results obtained by the Runge-Kutta method.

For the non-linear problem investigated, we can also see a lower accuracy of the one-cycle scheme and very close results obtained for the two-cycle scheme and the Crank-Nicholson method. Obviously, in the Crank-Nicholson method, the value of permissible error ε influences the accuracy of results (see results for $\varepsilon = 1e^{-6}$ and $\varepsilon = 1e^{-3}$).

Numerical efficiency of methods investigated can be defined by comparison of calculation time for the given time step and is presented in Fig. 11.

Fig. 11 shows that the two-cycle decomposition scheme is the method which requires the shortest calculation time. However, if we compare calculation time t_c in relation to number of equations, the best relation between accuracy of results and calculation time after including non-linear terms is obtained for the Runge-Kutta method. Calculation time t_c in relation to number of equations after including non-linear terms increases considerably for the two-cycle scheme. These results enable us to conclude that the Crank-Nicholson method is more universal than the two-cycle decomposition scheme.

5. Numerical case studies for a car park

The dispersion model presented in the paper can be used for numerical simulation of nitrogen oxides dispersion after cold start of vehicle engines and vehicle motion with unheated engines. The calculations are carried out for an open car park with dimensions as in Fig. 12. An inclination of wind angle $\alpha = 180°$ to axis $x^{(1)}$ is assumed.

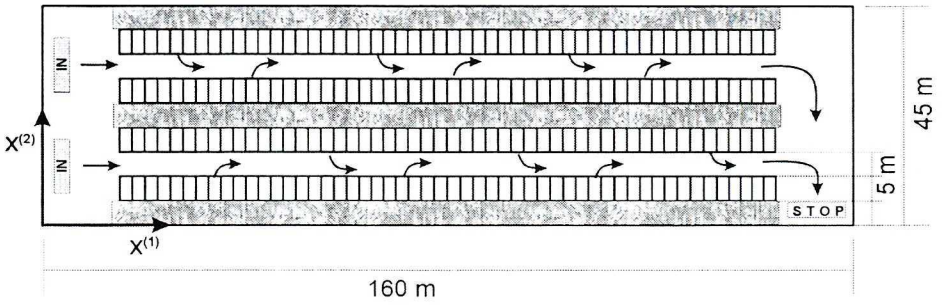

Fig. 12. Car park geometry

The domain investigated around the car park has the dimensions $360 \times 245 \times 10$ m. According to the finite volume method, the domain was divided into control volumes for $n_1 = 100$; $n_2 = 45$; $n_3 = 20$, so 90000 control volumes were obtained. In the calculations, Neumann boundary conditions were assumed for plane ($x^{(1)} = 360$) and plane ($x^{(3)} = 0$). Boundary Dirichlet conditions (which are used to describe free exchange between surroundings and domain) were assumed for the other boundaries of the domain. It was also assumed for simplification that initial concentration and background concentration at time $t_0 = 0$ are equal to zero.

The problem is to determine possible distributions of NO_2 and O_3 concentrations in the domain of the car park for given weather conditions. The input data were chosen in correspondence to a real situation. It was assumed that emission of nitrogen oxide was 95% of total emitted mass of nitrogen oxides. An unstable condition of atmosphere was taken into account in calculations with solar radiation equal to 940 W/m^2 (average radiation in June in Bielsko-Biała city). A numerical pre-processor was used in order to define data of wind profile and eddy diffusivity [2]. Input parameters for the pre-processor are presented in Table 1.

Table 1.

Input parameters for the pre-processor

Parameter	Value
Air velocity at height $x^{(3)} = 14$ *m*	3 m/s
Aerodynamic roughness	0.5 m
Ambient temperature at height $x^{(3)} = 2$ *m*	15°C
Ambient temperature at height $x^{(3)} = 14$ *m*	14.8°C
Atmospheric pressure	0.1 MPa

We modelled cars starting and leaving different parking spaces at random every 15 seconds over 30 minutes. Each car represented a moving source of pollutants in accordance with the multi-point model [2], [4].

Emission intensity for a vehicle of a given category which is inside control volume $V_{i,j,k}$ can be expressed as [2]:

$$I_{i,j,k} = \frac{1}{V_{i,j,k}} \left(\mathrm{ve}_{(l)}[\mathrm{v}] + \varepsilon_{(l)}(t, \mathrm{v}, T) \right) \tag{38}$$

where $e_{(l)}[\mathrm{v}]$ is road emission for a heated engine as a function of average vehicle velocity v for vehicle category l, $\varepsilon_{(l)}(t, \mathrm{v}, T)$ is intensity of additional

emission after cold start of vehicle engine in ambient temperature T and time of engine work after cold start t for given vehicle category I.

In simulation, it is assumed that each modelled vehicle remains stationary for the first ten seconds after the cold engine was started. After ten seconds the car accelerates to a velocity of about 30 km/h and leaves the car park by the shortest route. It stops at $x^{(2)} = 3$ to pay the parking charge. Then it exits the car park and the domain investigated.

The results obtained with the dispersion model presented can only be evaluated if calculations are based on statistical data which are representative for an actual car fleet. One method of creating a representative sample of cars in a car park is to divide vehicles up into commercial segments and note the percentage of each segment on market. If we then break down the total fleet according to cylinder capacity and SI/CI engine, we can find a classification as in Table 2 [2].

Table 2.

Assumed classification of SI and CI cars according to engine capacity

Type of engine	Engine capacity V_c [dm^3]		
	$V_c < 1.4$	$1.4 < V_c \leq 2.0$	$V_c > 2.0$
SI	49.2%	29.7%	21.1%
CI	–	62.4%	37.6%

The percentage distribution of cars according to pollutant emission and type of engine assumed in calculations is presented in Table 3.

Table 3.

Assumed percentage of cars fulfilling various legislation norms according to type of engine

Legislation Norm	Percentage of all fleet	Percentage in relation to type of engine [%]	
		SI	CI
Pre EURO	15	80	20
EURO 1	35	60	40
EURO 2	30	55	45
EURO 3	15	80	20
EURO 4	5	90	10

In order to determine emission from a vehicle of a given category, emission for a heated engine was calculated on the basis of the static characteristic (average road emission as a function of vehicle velocity)

according to the HBEFA model [15]. An example of characteristics of average road emission NOx as a function of average vehicle velocity is presented in Fig. 13.

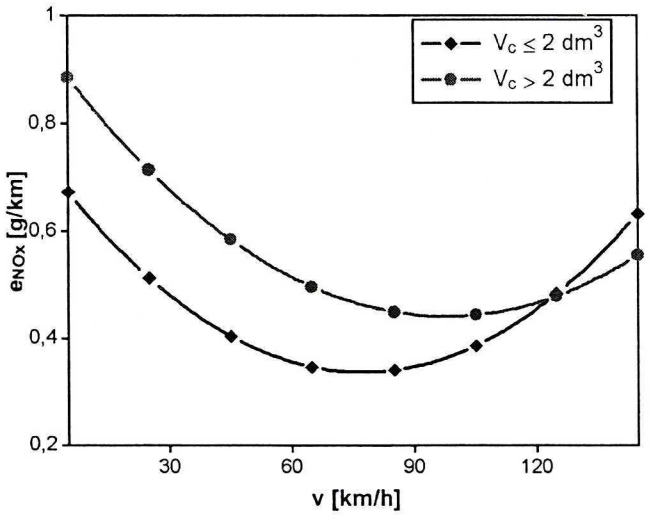

Fig. 13. Characteristics of average road emission of NO_x for vehicles with CI engine, fulfilling EURO II, in relation to engine capacity

Emission intensity for a vehicle of a given category after cold start was assumed as the power function of engine work presented in [2] according to the data from the INRETS model [16].

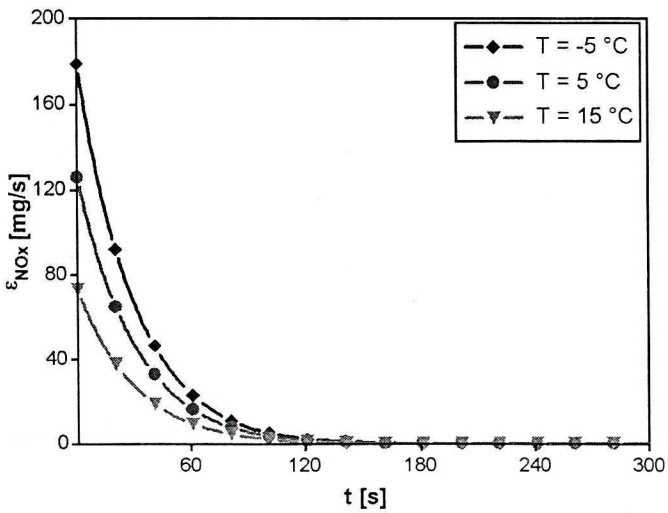

Fig. 14. Additional emission intensity characteristics of NO_x for vehicle with CI engine fulfilling EURO II, after cold start in various ambient temperatures

An example of additional emission intensity characteristics of NO_x, after cold start in various ambient temperatures for average velocity of vehicle v = 30 km/h, according to the data from the INRETS model, is presented in Fig. 14.

Numerical simulation of dispersion of emitted pollutants with chemical reactions enable us to calculate prognostic concentration of nitrogen oxides and concentration of ozone produced in chemical reactions as a secondary pollutant. Using the data given for atmospheric conditions, emission characteristics and car fleet, computer simulation gives us instantaneous and average concentrations of NO_2 and O_3 in the car park. Numerical calculations are carried out by the Crank-Nicholson method and a time step is equal to $\Delta t = 0.05$ s. The maximum values of calculated concentrations of nitrogen dioxide and ozone are presented in Table 4.

Table 4.
Maximum concentration of NO_2 and O_3 at a height of 1.8 m

Pollutant	ϕ_{max} [mg/m^3]
NO_2	0.059
O_3	$1.15 \cdot 10^{-4}$

Fig. 15 shows the average 30-minute distributions of NO_2 and O_3 concentration in the car park at a height of 1.8 m. Both concentrations are given in the scale $\log(\phi s)/\log(\phi_{max} s)$ where $s = 3 \cdot 10^8$.

The analysis of data presented in Table 4 and in Fig. 15 leads to the conclusion that, for the given simulation data, the calculated concentrations at a height of 1.8 m do not indicate that alarm values (which are defined as a 1-hour average) [17] would be exceeded, but it must be stressed that background concentration was assumed to be zero.

Apart from calculating averaged values, the numerical model of dispersion and multi-point source model presented can facilitate calculation of instantaneous concentrations at any height. Fig. 16 presents instantaneous concentrations of NO_2 and O_3 at the point with coordinates $x^{(1)} = 152.5$; $x^{(2)} = 3$; $x^{(3)} = 1.8$.

The results obtained by numerical simulation of the dispersion process and presented in the paper can be treated as an example of possible applications of numerical multi-point models in relation to car exhaust emission and dispersion. After taking into account other scenarios of car motion or different parameters of atmosphere, results obtained may be different to those presented.

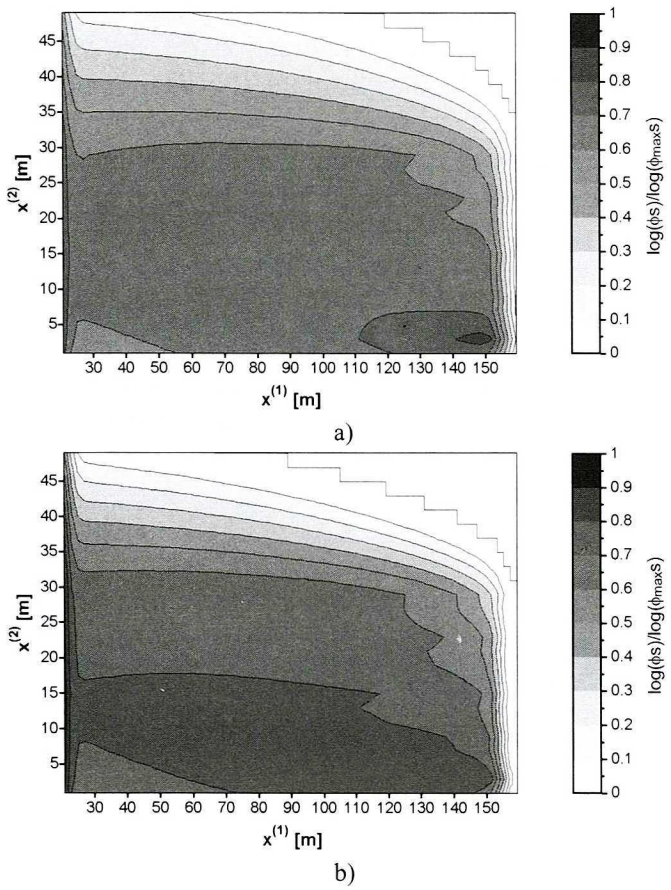

Fig. 15. Calculated average concentrations in car park at a height of 1.8 m
a) NO_2 b) O_3

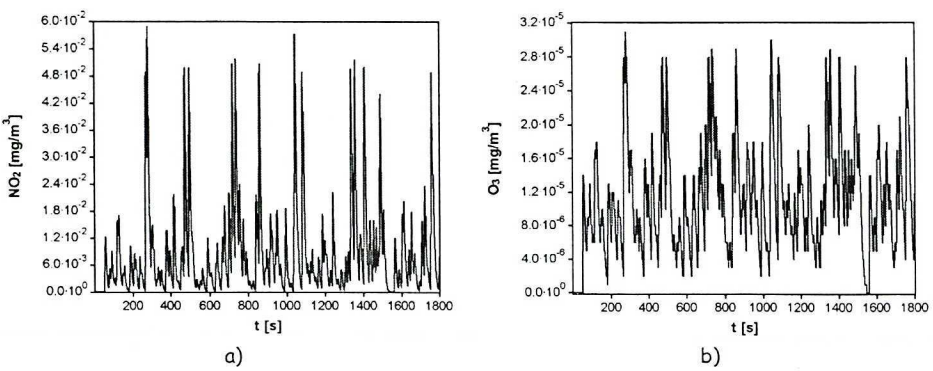

Fig. 16. Calculated instantaneous concentration for a) NO_2 b) O_3 in the car park (at point with coordinates $x^{(1)} = 152.5$; $x^{(2)} = 3$; $x^{(3)} = 1.8$)

6. Conclusion

The paper presents equations and computer models to carry out numerical simulations, in which we define vehicle pollutant concentrations. The model presented in the paper can be used in the analysis of dispersion of pollutants of vehicles travelling on roads and motorways or, as in the paper, around a car park. The mathematical model of pollutant dispersion phenomena consists of a linear partial differential equation for a single non-reactive pollutant or of a set of non-linear PDE if chemical reactions are included.

Numerical integration of a set of ordinary differential equations obtained after discretisation is possible by using a variety of methods. Numerical efficiency in solving dispersion problems by a classical method like the Runge-Kutta (IV order) and Crank-Nicholson is analysed in comparison to the decomposing one- and two-cycle schemes, which take into account a special form of ODE equations obtained after discretisation.

The simulations carried out enabled us to determine that the Crank-Nicholson method is a universal method, which can be applied to the problems of mass transport by advection and turbulent diffusion. The disadvantage of this method is the calculation time needed (longer in relation to the two-cycle scheme) for solution in the case of the linear advection-diffusion equation as a result of Gauss-Seidel iteration. It should be also underlined that decomposition schemes take into account the special form of operator $\mathbf{\Lambda}$ (equation (23)).

For numerical solution of a set of non-linear advection – diffusion equations, better results are given by the Crank-Nicholson method with Gauss-Seidel iterations instead of the decomposing two-cycle scheme. In this case, the set of ODE equations is stiff, and using the two-cycle scheme (with the same accuracy) is less numerically efficient than the Crank-Nicholson method.

On the basis of the results of simulation presented in the paper, we can state that for a non-linear dispersion problem a smaller integration time step should be used than for linear dispersion problems. Where a large number of equations are conjugate, the Runge-Kutta or Crank-Nicholson method with Gauss-Seidel iteration should be used.

This paper was written as part of Project 4 T12D 008 26 financed by the Committee for Scientific Research.

Manuscript received by Editorial Board, September 08, 2004;
final version, February 10, 2005.

REFERENCES

[1] Chłopek Z. : Ochrona środowiska naturalnego. WKŁ, Warszawa, 2002.
[2] Brzozowska L., Brzozowski K. : Komputerowe modelowanie emisji i rozprzestrzeniania się zanieczyszczeń samochodowych. Śląsk, Katowice-Warszawa, 2003.
[3] Brzozowski K., Romaniszyn K.: An effective method of creating dynamic characteristics using drive tests. Archiwum Budowy Maszyn, Vol. L, 2003, pp. 391÷408.
[4] Brzozowska L., Brzozowski K., Wojciech S.: Computational Modelling of car Pollutant Dispersion. Śląsk, Katowice, 2001.
[5] Chapra S. C., Canale R. P. : Numerical methods for engineers. McGraw-Hill Higher Education. New York, 2002.
[6] Marczuk G. I.: Modelowanie matematyczne problemów środowiska naturalnego. PWN, Warszawa 1985.
[7] Gryboś R.: Podstawy mechaniki płynów. PWN, Warszawa, 1998.
[8] Shaw C. T.: Using Computational Fluid Dynamics. Prentice Hall, 1992.
[9] Legras J.: Praktyczne metody analizy numerycznej. WNT, Warszawa, 1974.
[10] Ralston A.: Wstęp do analizy numerycznej. Warszawa, 1971.
[11] Lomax H., Pulliam T. H., Zingg D.: Fundamentals of Computational Fluid Dynamics. Springer Verlag, 1999.
[12] Berkowicz R., Hertel O., Larsen S. E., Srensen N. N., Nielsen M.: Modelling traffic pollution in streets. Ministry of Environment and Energy. National Environmental Research Institute, Denmark, 1997.
[13] Zannetti P.: Air pollution modeling. Theories, computational methods and available software. Van Nostrand Reinhold, New York, 1990.
[14] Kukkonen J., Wallenius L., Karppinen A., Pohjola M., Dorling S., Chatterton T., Ruuskanen J., Kolehmainen M., Junninen H., Ruuskanen A: Literature review on nitrogen oxides modelling at a point. APPETISE (IST-99-11764) Project report, 2001.
[15] Handbook Emission Factors for Road Transport. Version 1.2, INFRAS, 1999.
[16] Joumard R., Serie E.: Modelling of cold start emissions for passenger cars. INRETS report LTE 9931, 1999.
[17] Załącznik nr 4 do rozporządzenia Ministra Środowiska z dnia 5 grudnia 2002 r. (Dz. U. Nr 1, poz. 12. 2003 r.).

Numeryczne modelowanie dyspersji zanieczyszczeń pochodzenia motoryzacyjnego z uwzględnieniem przemian chemicznych

Streszczenie

W artykule przedstawiono model dyspersji zanieczyszczeń emitowanych przez silniki spalinowe pojazdów, umożliwiający ocenę stopnia oddziaływania transportu na środowisko. Model numeryczny dyspersji sformułowano przy zastosowaniu metody objętości skończonych. Przedstawiono równania uzyskane w wyniku dyskretyzacji zagadnienia oraz omówiono metody ich rozwiązania (metodą Rungego-Kutty, Cranka-Nicholsona oraz dekompozycji). Na podstawie przeprowadzonych symulacji komputerowych podano wnioski dotyczące efektywności numerycznej poszczególnych metod. Sformułowano zadanie dyspersji tlenków azotu (NO_x) z uwzględnieniem przemian chemicznych i przedstawiono wyniki symulacji komputerowych. W zadaniu uwzględniono także zwiększoną emisję w warunkach zimnego rozruchu silników.